EUKARYOTIC CELL, Apr. 2009, p. 640–648 Vol. 8, No. 4
1535-9778/09/$08.00+0 doi:10.1128/EC.00347-08

Disruption of *Plasmodium* Sporozoite Transmission by Depletion of Sporozoite Invasion-Associated Protein 1▽§

Sabine Engelmann,[1]† Olivier Silvie,[1,2]† and Kai Matuschewski[1,2]*

Department of Parasitology, Heidelberg University School of Medicine, 69120 Heidelberg, Germany,[1] and Parasitology Unit, Max Planck Institute for Infection Biology, 10117 Berlin, Germany[2]

Received 16 October 2008/Accepted 15 January 2009

Accumulation of infectious *Plasmodium* sporozoites in *Anopheles* spp. salivary glands marks the final step of the complex development of the malaria parasite in the insect vector. Sporozoites are formed inside midgut-associated oocysts and actively egress into the mosquito hemocoel. Traversal of the salivary gland acinar cells correlates with the sporozoite's capacity to perform continuous gliding motility. Here, we characterized the cellular role of the *Plasmodium berghei* sporozoite invasion-associated protein 1 (SIAP-1). Intriguingly, *SIAP-1* orthologs are found exclusively in apicomplexan hemoprotozoa, parasites that are transmitted by arthropod vectors, e.g., *Plasmodium*, *Babesia*, and *Theileria* species. By fluorescent tagging with mCherry, we show that SIAP-1 is expressed in oocyst-derived and salivary gland-associated sporozoites, where it accumulates at the apical tip. Targeted disruption of *SIAP-1* does not affect sporozoite formation but causes a partial defect in sporozoite egress from oocysts and abolishes sporozoite colonization of mosquito salivary glands. Parasites with the *siap-1*(−) mutation are blocked in their capacity to perform continuous gliding motility. We propose that arthropod-transmitted apicomplexan parasites specifically express secretory factors, such as SIAP-1, that mediate efficient oocyst exit and migration to the salivary glands.

Protozoan parasites of the phylum *Apicomplexa* have adopted an obligate intracellular life-style in a wide range of animal hosts. Apicomplexan parasites share many characteristics, including a set of apical specialized secretory organelles, active substrate-dependent locomotion, and compartmentalization of biosynthetic pathways in apicoplasts. Transmission to the vertebrate hosts occurs via tailor-made motile parasite stages, termed sporozoites, which are formed inside oocysts, the only extracellular replication phase during the complex apicomplexan life cycles. However, apicomplexan parasites differ fundamentally in their transmission modes. Coccidian parasites, such as *Toxoplasma gondii*, the causative agent of toxoplasmosis, and cryptosporidia, which can cause life-threatening diarrhea, form oocysts that are taken up orally via contaminated food or water, respectively. After accidental ingestion, sporozoites are liberated from the oocysts and breach or directly invade the intestinal endothelium to commence an infection. In marked contrast, sporozoites of apicomplexan hemoprotozoa are inoculated intradermally by arthropod vectors, e.g., *Anopheles* mosquitoes or ticks. Sporozoites then actively leave the inoculation site and enter the blood circulation (3). In the case of *Plasmodium* species, the causative agents of malaria, sporozoites are formed in midgut-associated oocysts (16), actively exit the oocyst (1, 23), and penetrate the distal portion of the lateral salivary gland lobes where they eventually accumulate, rendering the infected mosquito infectious to the vertebrate host (4).

Colonization of the salivary glands by *Plasmodium* parasites is driven by a number of stage-specific surface proteins (9), including (i) the major sporozoite surface protein circumsporozoite protein (CSP) (18), (ii) the sporozoite adhesin apical membrane antigen/erythrocyte binding-like protein (MAEBL) (8), and (iii) the sporozoite invasin thrombospondin-related anonymous protein (TRAP) (7, 10, 17, 24). However, none of these proteins are conserved across apicomplexan hemoprotozoa, indicating a high degree of parasite/invertebrate host coadaptation. Toward a better understanding of the basic molecular mechanisms of sporozoite motility and arthropod-mediated transmission, we searched for sporozoite-specific candidates that are shared between *Plasmodium* spp., *Babesia* spp., and *Theileria* spp.

SIAP-1/*ag17*/*S5* (PFD0425w) was first discovered in a systematic screen for *Plasmodium falciparum* sporozoite antigens recognized by sera from individuals that were immunized with irradiated sporozoites and termed antigen 17 (ag17) (2). Subsequently, the *Plasmodium yoelii* ortholog was isolated in a suppression subtractive hybridization screen for genes that are specifically upregulated in sporozoites compared to blood stages (6). More recently, the *P. falciparum* ortholog was identified as a gene that is transiently upregulated in activated *P. falciparum* sporozoites (14).

In this study, we fluorescently tagged the *Plasmodium berghei SIAP-1* gene (Pb*SIAP-1*) and show enrichment of the protein in the apical pole of the sporozoite. Targeted gene deletion resulted in viable blood stage parasites that displayed a specific and complete block in sporozoite transmission to the vertebrate host.

* Corresponding author. Mailing address: Parasitology Unit, Max Planck Institute for Infection Biology, Charitéplatz 1, 10117 Berlin, Germany. Phone: 49-30-28460535. Fax: 49-30-28460225. E-mail: matuschewski@mpiib-berlin.mpg.de.

† These authors contributed equally.

§ Supplemental material for this article may be found at http://ec.asm.org/.

▽ Published ahead of print on 30 January 2009.

MATERIALS AND METHODS

Experimental animals. Animals were from Charles River Laboratories. All animal work was conducted in accordance with European regulations and approved by the state authorities (Regierungspräsidium Karlsruhe).

Reverse transcriptase PCR (RT-PCR). Total RNA was purified from *Plasmodium berghei* ANKA (GFP507cl1)-infected mosquito midguts (oocysts), salivary glands (sporozoites), and infected HepG2 cells (early liver stages) or mouse erythrocytes (mixed blood stages) using the RNeasy kit (Qiagen). Reverse transcription was performed using the RETROscript kit (Ambion). Real-time quantitative PCR was performed on cDNA preparations using the ABI 7500 sequence detection system and Power SYBR green PCR master mix (Applied Biosystems), according to the manufacturer's instructions. Quantitative PCR was performed in triplicate, with 1 cycle of 95°C for 15 min, followed by 40 cycles of 95°C for 15 s, 55°C for 15 s, and 60°C for 45 s. Standard curves were generated for all primers using wild-type (WT) cDNA serial dilutions and gave amplification efficiencies of 90 to 100%. Data were analyzed with SDS 1.3.1 software (Applied Biosystems). Relative transcript abundance was normalized to the *GFP* gene, which is constitutively expressed in *P. berghei* ANKA GFP507cl1 (5). The following primers were used for real-time PCR: *GFP* forward (5′-GATGGAAGCGTTCAACTAG CAGACC-3′), *GFP* reverse (5′-AGCTGTTACAAACTCAAGAAGGACC-3′), *SIAP-1* forward (5′-CAGCAATTAGGGACAGTGATGG-3′), *SIAP-1* reverse (5′-AATAATGGACACCTCCGTGTGG-3′), *HSP70* forward (5′-TGCAGCAGATA ATCAAACTC-3′), and *HSP70* reverse (5′-ACTTCAATTTGTGGAACACC-3′).

Generation of the mCherry-tagged *SIAP-1* parasite line. For targeted fluorescent tagging of Pb*SIAP-1*, a fragment corresponding to the 3′ end of the Pb*SIAP-1* open reading frame (ORF) without the stop codon was amplified by PCR using *P. berghei* genomic DNA as the template and primers mCherry-*SIAP-1*for (5′-ATAAGAATGCGGCCGCGCATCTGAAAGTAAAGGAAAATGGGTC GC-3′; NotI site is underlined) and mCherry-*SIAP-1*rev (5′-GGGCTAGCTGA ATTGTCCACGAAAACACTGTAACTATAGG-3′; NheI site is underlined). The PCR product was cloned into the B3D+mCherry vector (15) immediately upstream of the mCherry sequence and the Pb*DHFR/TS* 3′ untranslated region (UTR), resulting in the *SIAP-1*/*mCherry* targeting plasmid. The *SIAP-1*/*mCherry* plasmid was linearized with SpeI, and parasite transfection, positive selection, and parasite cloning were performed as described previously (5). Integration-specific PCR amplification of the mCherry-tagged *SIAP-1* was generated using specific primer combinations. We obtained one parasite population that was used for a systematic expression and localization analysis. Expression of the mCherry fusion proteins was analyzed through direct detection of the red fluorescence of mCherry by confocal microscopy. Images were acquired on a Zeiss LSM510 confocal system (Zeiss, Germany) and processed with Adobe Photoshop software (Adobe Systems, Inc.).

Generation of the *siap-1*(−) parasites. For targeted disruption of the *SIAP-1* gene, two PCR fragments flanking the *SIAP-1* ORF were amplified from genomic *Plasmodium berghei* DNA. The 5′ UTR amplification with the primer combination 5′SIAP-1-Rep_for (5′-GGGGTACCGTGTTTTCATGCTATATG TACATTTGC-3′; KpnI site is underlined) and 5′SIAP-1-Rep_rev (5′-CCCAA GCTTGATGATATTGACCGTAAAATCC-3′; HindIII site is underlined) resulted in a 634-bp 5′ UTR fragment. Cloning into the standard *P. berghei* transfection vector b3D.DTˆH.ˆD resulted in pSE-41. Next, a 788-bp 3′ UTR fragment was amplified with primers 5′SIAP-1-Rep_ for (5′-CGGGATCCCCT ATAGTTACAGTGTTTTCG-3′; BamHI site is underlined) and 5′SIAP-1-Rep_ rev (5′-GGACTAGTGTTCGATATACCTTGCAGATTCC-3′; SpeI site is underlined) and cloned into pSE-41. This resulted in the *SIAP-1* targeting vector pSE-65, which contained both fragments flanking the positive selection marker *T. gondii* dihydrofolate reductase/thymidylate synthase (*dhfr/ts*), allowing replacement of the endogenous *SIAP-1* locus upon a double crossover event and subsequent selection with the antifolate pyrimethamine (19). *P. berghei* transfection was done with 10 μg KpnI/SpeI-digested pSE-65 and gradient-purified *P. berghei* NK65 and *P. berghei* ANKA (clone GFP507cl1) schizonts (5). Positive selection for successful integration of the targeting plasmid was carried out by providing 70 μg/ml pyrimethamine with the drinking water for a period of 8 days. Transfer of the emerging *P. berghei* population into naive animals confirmed pyrimethamine resistance. Genomic DNAs for selected parasite populations were genotyped by an integration-specific PCR using primers Tgfor (5′-CCCG CACGGACGAATCCAGATGG-3′) and SIAP-1_int_check2_rev (5′-CTGTGA ATGTGTATATTGTGCATATGCC-3′). Clonal *siap1*(−) parasite populations were obtained by limiting dilution into 15 naive NMRI mice and confirmed by integration-specific PCR.

As a complementary approach, we generated *SIAP-1* knockout parasites specifically expressing green fluorescent protein (GFP) in sporozoites. For this purpose, we first amplified by PCR a fragment comprising the *CSP* promoter region and the *GFP* coding sequence, using primers GFPfor (5′-ATAAGAAT GCGGCCGCGACATGCATATGTGTTGGTTGTAATTGAGG-3′; NotI site is underlined) and GFPrev (5′-CGCGGATCCTTATTTGTATAGTTCATCCA TGCC-3′; BamHI site is underlined) and genomic DNA from the PbFluspo parasite line (11) as a template. Cloning of this fragment into the B3D+ vector (15) using NotI/BamHI resulted in the vector B3D+CSPGFP. 5′ and 3′ fragments of the Pb*SIAP-1* gene were then amplified using primers SIAP-1_REP1 (5′-TCCCCGCGGAGTTAACTCGAAAAAAATAAGGACG-3′; SacII site is underlined) and SIAP-1_REP2 (5′-ATAAGAATGCGGCCGCTTTTAAGATATAC CCCTTAATGAGAGC-3′; NotI site is underlined) and primers SIAP-1_REP3 (5′-CCCAAGCTTGATGTATGTATAATACCGAAAATTGG-3′; HindIII site is underlined) and SIAP-1_REP4 (5′-CGGGGTACCCGCCTTATTTAAGGGATA AAGAATGGG-3′; KpnI site is underlined), respectively, and genomic DNA from WT *P. berghei*. These two fragments were then cloned into the B3D+CSPGFP vector, using the respective restriction endonucleases to generate the targeting construct SIAP-1-GFPrep. Transfection, selection, and cloning were then performed as described above. Genotyping PCR using specific primer combinations confirmed the expected recombination event.

Phenotypical analysis during the *Plasmodium* life cycle in vivo. Blood stage development was analyzed in vivo in asynchronous infections using NMRI mice. Gametocyte differentiation and exflagellation of microgametes were detected in mice before mosquito feedings. *Anopheles stephensi* mosquito rearing and maintenance was carried out under a 14 h light/10 h dark cycle with 75% humidity at 28°C. Once infected, *Anopheles* mosquitoes were kept at 80% humidity and 20°C. Sporozoite populations were separated and analyzed as described previously (21). Briefly, for determination of sporozoite infectivity and numbers of midgut- and salivary gland-associated sporozoites, infected mosquitoes were dissected at days 10, 14, and 17 after feeding, respectively. Hemocoel sporozoites were recovered at days 14, 16, and 18 after feeding. For determination of infectivity, sporozoites isolated from mosquito midguts, hemocoel, or salivary glands were injected intravenously at the numbers indicated into young Sprague-Dawley rats. Patency was checked daily by microscopic examination of Giemsa-stained blood smears.

In vitro experiments. For analysis of gliding motility, sporozoites isolated from infected mosquito salivary glands were deposited on glass slides coated with bovine serum albumin and incubated at 37°C for 30 min. Trails left behind gliding parasites were then visualized using anti-CSP antibodies (12), followed by anti-mouse Alexa Fluor 488 antibodies (Molecular Probes). For analysis of exoerythrocytic form development, we used HuH7 cells cultured in Dulbecco's modified Eagle's medium supplemented with 10% fetal calf serum and antibiotics. *P. berghei* sporozoites were added in triplicate wells, incubated for 2 h at 37°C, and washed off. After 48 h, exoerythrocytic forms were revealed using primary antibodies against *Plasmodium* heat shock protein 70 (HSP70) (20), followed by the anti-mouse Alexa Fluor 488 secondary antibody. In vitro analysis of the Pb*SIAP-1*/*mCherry* parasites was performed in HepG2 cells, as described previously (15).

RESULTS

***SIAP-1* is conserved in arthropod-transmitted *Apicomplexa* spp. and is specifically expressed in *P. berghei* mosquito stages.** We initiated our characterization of *SIAP-1*/*ag17*/*S5* by an in silico analysis of orthologous genes in *Plasmodium* species and related apicomplexan parasites (Fig. 1A). The *SIAP-1* genes from the model rodent-infecting *Plasmodium* species *P. yoelii* and *P. berghei* encode proteins of 999 amino acid residues each. *SIAP-1* members appear to be potentially secreted proteins and are readily retrieved from annotated *Plasmodium* genomes. Remarkably, *SIAP-1* orthologs are present in the *Babesia* and *Theileria* genomes (see Fig. S1 in the supplemental material) but absent in *Toxoplasma* and *Cryptosporidium*, indicating that its presence may be restricted to arthropod-transmitted apicomplexan parasites (Fig. 1A). Analysis of SIAP-1 protein sequence indicates the presence of a signal peptide but no identified conserved domain (see Fig. S1 in the supplemental material).

We next analyzed *SIAP-1* transcript abundance during sporozoite maturation in the rodent malaria model parasite *P.*

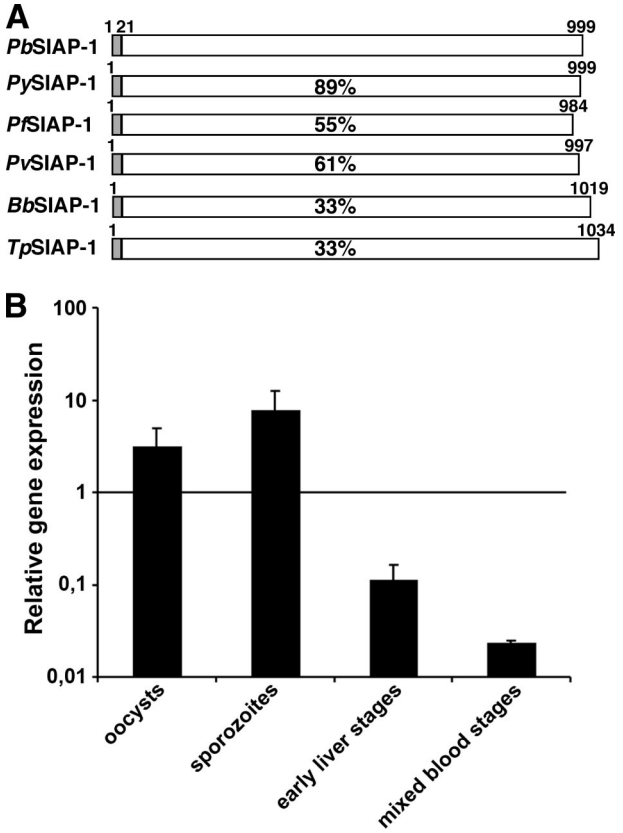

FIG. 1. *Plasmodium* SIAP-1. (A) Schematic diagram of the primary structures of the apicomplexan SIAP-1 proteins. The primary structure of *P. berghei* SIAP-1 (PB000251.01.0; reannotated) and the orthologs of *P. yoelii* (PY00455), *P. falciparum* (PFD0425w), *Plasmodium vivax* (Pv000815), *Babesia bovis* (XP_001609197), and *Theileria parva* (XP_765499) are indicated with white boxes. The predicted cleavable signal peptide is represented in gray. Amino acid sequence identities are indicated as percentages of identical residues compared to the *P. berghei* sequence. (B) Quantitative RT-PCR analysis of *P. berghei SIAP-1* gene expression in midgut oocysts (day 12 postinfection of mosquitoes), salivary gland sporozoites (day 18 postinfection of mosquitoes), early liver stages (6 h postinfection of HepG2 cells) and mixed blood stages. Relative gene expression was normalized to *GFP* expression level and is shown as the mean (± standard deviation) of the results from two independent experiments.

berghei. cDNAs generated from asexual blood stages, liver stages, oocysts, and salivary gland-associated sporozoites were used as templates for quantitative RT-PCR (Fig. 1B). Pb*SIAP-1* expression was highest in young oocysts and sporozoites and rapidly decreased after sporozoite invasion of hepatocytes. In good agreement with data obtained using *P. yoelii* (6), expression of Pb*SIAP-1* was very low in blood stages. Collectively, *SIAP-1* expression correlates with a presumed role in the arthropod vector.

Pb*SIAP-1* is localized at the apical tip and the surface of sporozoites. In order to investigate the cellular localization and the expression timing of Pb*SIAP-1*, we generated parasite lines expressing the endogenous SIAP-1 protein fused to the mCherry red fluorescent protein (13). This was achieved by transfection of a targeting vector that contains an amino-terminally truncated Pb*SIAP-1* copy and in-frame fusion of the mCherry coding region, followed by the *DHFR*/*TS* 3′ UTR (see Fig. S2A in the supplemental material). Upon a single crossover event, integration of this construct is predicted to result in an allelic duplication (19), resulting in an mCherry-tagged full-length copy and a nontranscribed 5′ truncated version of the Pb*SIAP-1*. Transfection was performed in *P. berghei* ANKA parasites expressing GFP (5), leading to green fluorescent parasites that express a red fluorescent SIAP-1 protein. Genotyping by PCR using specific primer combinations confirmed the desired integration event (see Fig. S2B in the supplemental material). Importantly, Pb*SIAP-1*/*mCherry* parasites completed the parasite life cycle normally. They were indistinguishable from WT parasites in development and growth of asexual stages (data not shown). Pb*SIAP-1*/*mCherry* parasites produced gametocytes, and exflagellation of male gametocytes was similar to that in WT parasites (data not shown). Transmission to *Anopheles stephensi* mosquitoes and oocyst development were also normal compared to WT parasites. Pb*SIAP-1*/*mCherry* oocysts produced sporozoites, which invaded mosquito salivary glands. In two independent infection experiments, we found 20,000 and 16,700 salivary gland-associated sporozoites per mosquito, respectively, numbers which are similar to those obtained with WT parasites (see Fig. 4D). More importantly, Pb*SIAP-1*/*mCherry* sporozoites were infective as demonstrated by complete liver stage development in vitro (Fig. 2E) and in vivo. C57/BL6 mice inoculated intravenously with 5,000 Pb*SIAP-1*/*mCherry* sporozoites ($n = 5$) or exposed to the bites of five infected mosquitoes ($n = 5$) all developed a patent parasitemia at day 3 or day 4 after inoculation, respectively, similar to those infected with WT parasites. Collectively, these data demonstrate that the C-terminal tagging of SIAP-1 had no detrimental effect on *P. berghei* infectivity.

We first performed live cell imaging of blood stages of the transgenic Pb*SIAP-1*/*mCherry*. In good agreement with our transcription analysis and published data (6), we could not detect a red signal throughout the blood stage development of the malaria parasite (data not shown). In contrast, the fusion protein was abundantly expressed in oocyst-derived and salivary gland sporozoites (Fig. 2A and B). Remarkably, in both immature and mature sporozoites, Pb*SIAP-1*/*mCherry* showed a polarized distribution predominant at the apical tip of the parasites, as confirmed by examination of motile sporozoites (Fig. 2C). Interestingly, in addition to this apical concentration, Pb*SIAP-1*/*mCherry* was also detected as distinct patches distributed along the parasite (Fig. 2C). These patches were sometimes clearly distributed at the periphery of the parasite, suggesting a possible association of *SIAP-1* with the sporozoite pellicle (Fig. 2D). This pattern is consistent with immunofluorescence data generated with antibodies against *P. falciparum* SIAP-1 (14). Interestingly, we observed no change in the distribution of Pb*SIAP-1*/*mCherry* during the gliding of motile sporozoites (Fig. 2C).

We further examined the fate of Pb*SIAP-1*/*mCherry* after sporozoite invasion of HepG2 hepatocytic cells. In transforming sporozoites 4 h postinfection, Pb*SIAP-1*/*mCherry* was detected in distinct patches, without clear apical polarization (Fig. 2E). These dotted structures were still detected 24 h postinfection, although at a lower intensity, but had completely disappeared in mature liver stages 72 h postinfection (Fig. 2E),

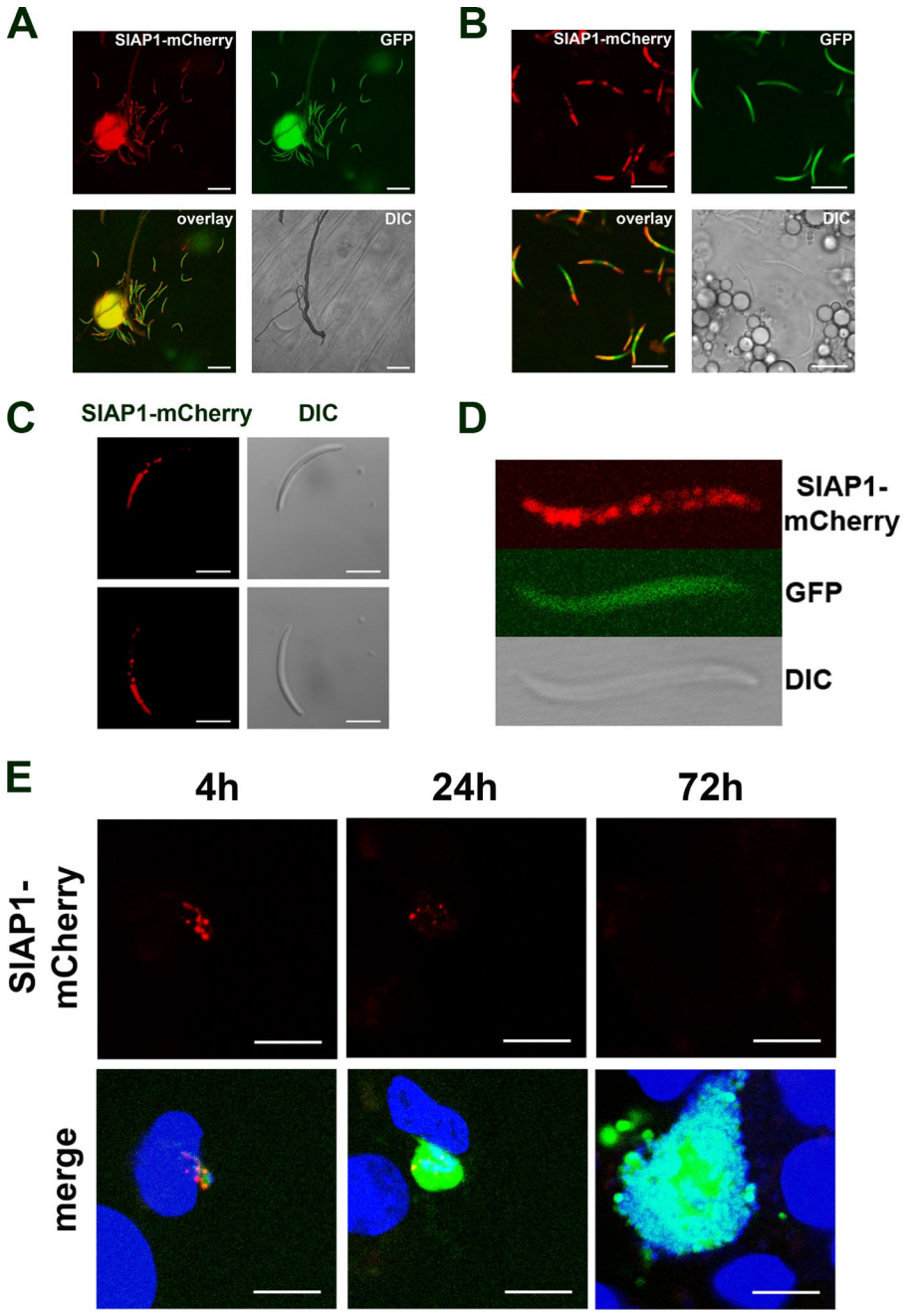

FIG. 2. Expression and localization of Pb*SIAP-1/mCherry* in sporozoites. Expression of the mCherry-tagged SIAP-1 (red) was analyzed by confocal fluorescence microscopy of SIAP-1/mCherry *P. berghei* parasites constitutively expressing GFP (green). (A) Midgut sporozoites. Bar, 20 μm. (B) Salivary gland-associated sporozoites. Bar, 10 μm. (C) Fluorescent imaging of a motile sporozoite. Sequential acquisition of the red fluorescence and differential interference contrast (DIC) confirms SIAP-1 accumulation mainly at the apical tip. Note that the distribution of SIAP-1/mCherry is not modified as the sporozoite glides. Bar, 5 μm. (D) Higher magnification of a fixed salivary gland-associated sporozoite. (E) Confocal microscopy analysis of HepG2 cell cultures 4 h, 24 h, and 72 h after infection with *P. berghei* parasites expressing GFP (green) and SIAP-1/mCherry (red). Nuclei were stained with Hoechst 33342 (blue). Bars, 10 μm.

consistent with the absence of Pb*SIAP-1/mCherry* expression observed in blood stages.

Generation of Pb*SIAP-1* knockout parasites. To address the function of *SIAP-1* during the *Plasmodium* life cycle, we generated loss-of-function *P. berghei* parasites. We used a replacement strategy (Fig. 3A) to disrupt the endogenous *SIAP-1* gene copy by double-crossover homologous recombination (19). A targeting construct comprising 5′ and 3′ fragments of *SIAP-1* flanking the pyrimethamine resistance cassette was used for positive selection after parasite transfection. The parental blood stage population from a successful transfection was used to isolate one disruptant clone, which was subsequently used for phenotypical analysis. Occurrence of the double crossover was confirmed by PCR in pyrimethamine-resistant parasites,

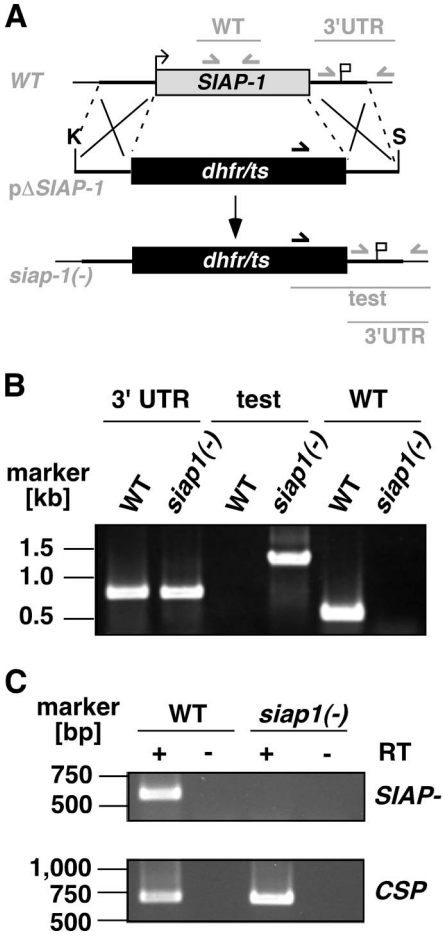

FIG. 3. Targeted deletion of the *P. berghei SIAP-1* gene. (A) Replacement strategy for targeted gene disruption of Pb*SIAP-1*. The WT *SIAP-1* locus (WT) is targeted with a KpnI (K)/SpeI (S)-linearized replacement plasmid (pΔ*SIAP-1*) containing the 5′ and 3′ UTR of Pb*SIAP-1* and the positive selection marker *TgDHFR-TS*. After double-crossover homologous recombination, the *SIAP-1* ORF is substituted by the selection marker, resulting in the mutant *siap-1*(−) allele. Replacement- and WT-specific test primer combinations and expected fragments are shown as lines. (B) Replacement-specific PCR analysis. Confirmation of the predicted gene targeting is done with primer combinations that amplify only a signal in the recombinant locus (test). The absence of a WT-specific signal in the clonal *siap-1*(−) parasite population confirms the purity of the mutant parasite line. (C) Depletion of *SIAP-1* transcripts in *siap-1*(−) parasites. cDNA from WT and *siap-1*(−) sporozoites were used as a template for *SIAP-1*-specific PCRs (top). Amplification of the circumsporozoite protein (*CSP*) transcripts was used as a positive control (bottom).

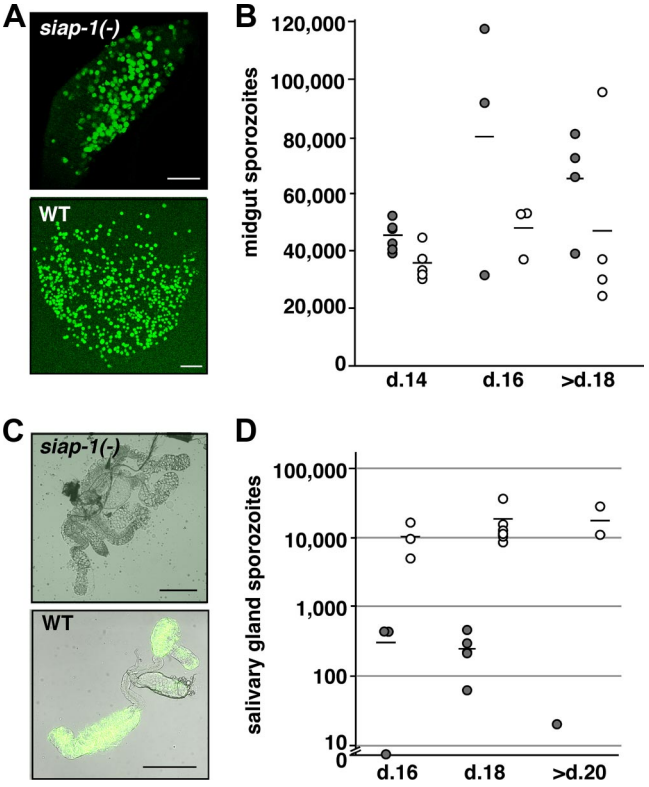

FIG. 4. *siap-1*(−) sporozoites are impaired in egress from oocysts. (A) Representative immunofluorescence pictures of infected *A. stephensi* midguts at day 14 after infection. (B) Quantification of oocyst-associated sporozoites per infected mosquito for *siap-1*(−) (gray circles) and WT (white circles) parasites. The bars represent the mean values. (C) Representative merged bright field and immunofluorescence pictures of infected *A. stephensi* salivary glands at day 17 after infection. (D) Quantification of salivary gland-associated sporozoites per infected mosquito for *siap-1*(−) (gray circles) and WT (white circles) parasites. Note the logarithmic scale. Bars, 200 μm.

using primers specific for the recombination event (Fig. 3B). The WT locus was not detected in *siap-1*(−) parasites, confirming the homogeneity of the expected recombination. While *CSP* control transcripts were detected in WT as well as *siap-1*(−) sporozoites by RT-PCR, *SIAP-1* transcripts were detected only in WT, but not in *siap-1*(−) sporozoites, confirming the successful depletion of *SIAP-1* in the mutants (Fig. 3C).

Pb*SIAP-1* is required for infection of mosquito salivary glands and transmission to the mammalian host. We next examined the phenotype of *siap-1*(−) parasites during the *P. berghei* life cycle. As expected from successful disruption of the *SIAP-1* gene in blood stages, *siap-1*(−) parasites were indistinguishable from WT parasites in development and growth of asexual stages (data not shown). *SIAP-1*-deficient parasites produced gametocytes, and exflagellation of male gametocytes was similar to that in WT parasites (data not shown). These data demonstrate that *SIAP-1* is not required during asexual blood stage development and sexual differentiation.

We next investigated transmission of *SIAP-1* knockout parasites to *Anopheles stephensi* mosquitoes. We let mosquitoes feed on mice infected with *siap-1*(−) or WT parasites, and at different time points after the blood meal, mosquitoes were dissected and examined for parasite development. Examination at days 10 and 14 demonstrated that *siap-1*(−) parasites formed high numbers of oocysts and oocyst-derived sporozoites, respectively, as did WT parasites (Fig. 4A and B). We noticed a persistence of high numbers of midgut-associated sporozoites per infected mosquito beyond day 18 after infection (Fig. 4B). Strikingly, at day 16 after mosquito feeding, the number of *siap-1*(−) sporozoites associated with salivary glands was dramatically reduced compared to that of WT parasites (Fig. 4C and D). This defect was also observed when salivary glands were examined later, beyond day 20. These

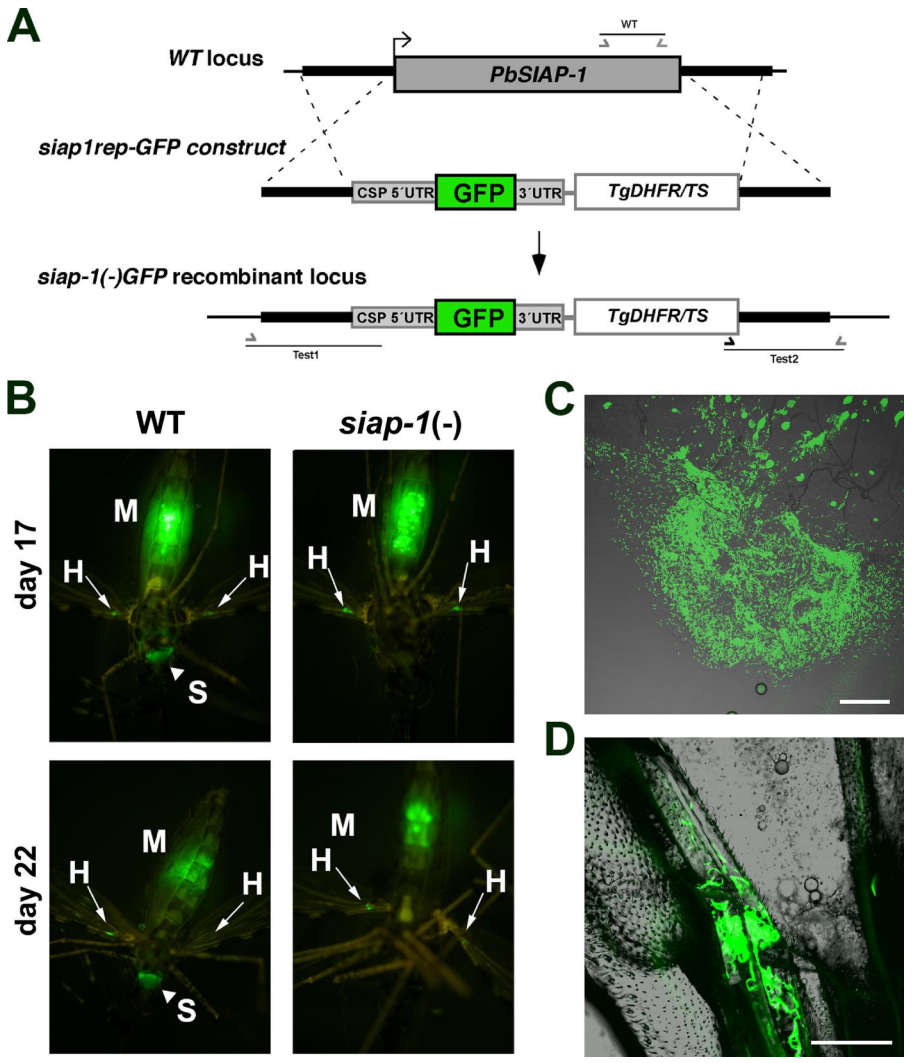

FIG. 5. *siap-1*(−) sporozoites fail to colonize the mosquito salivary glands. (A) Replacement strategy for targeted gene disruption of Pb*SIAP-1* and insertion of a *GFP* expression cassette. The WT *SIAP-1* locus is targeted with a SacII/KpnI-linearized replacement plasmid (*siap1rep-GFP* construct) containing the 5′ and 3′ UTR of Pb*SIAP-1*, the positive selection marker *TgDHFR-TS*, and the *GFP* coding sequence under the control of the *CSP* promoter region. After double crossover homologous recombination, the *SIAP-1* ORF is substituted by the selection marker and the *GFP* cassette, resulting in the mutant *siap-1*(−)/*GFP* allele. (B) Fluorescence imaging of whole mosquitoes infected with WT or *siap-1*(−)/*GFP* parasites, day 17 and day 22 after the infectious blood meal. Note the presence of green fluorescent WT parasites in the mosquito midgut (M), hemocoel (H, best visualized in the wings with arrows), and salivary glands (S, arrowheads). *siap-1*(−)/*GFP* parasites were only detected in the midgut (M) and the hemocoel (H, arrows), but not in salivary glands of infected mosquitoes. (C) Fluorescence microscopy of a dissected mosquito midgut 21 days after infection with *siap1*(−)/*GFP* parasites. Note the presence of oocysts and the release of high numbers of sporozoites. Bar, 200 μm. (D) Fluorescence microscopy of a dissected mosquito wing 21 days after infection with *siap-1*(−)/*GFP* parasites, demonstrating the presence of sporozoites in the hemocoel. Bar, 50 μm.

results indicate that *siap-1*(−) sporozoites have a defect in the egress from oocysts and/or the invasion of salivary glands.

To discriminate between these two possibilities, we performed in vivo imaging of whole infected mosquitoes. For this purpose, we generated an additional *SIAP-1*-deficient line using a replacement cassette containing the *GFP* coding sequence under the control of the *CSP* promoter, cloned in tandem with the positive selection marker *Tgdhfr/ts* (Fig. 5A). After integration of this construct in recombinant *P. berghei* parasites, we obtained a *siap-1*(−)/*GFP* parasite line, characterized by deletion of the *SIAP-1* gene (see Fig. S3 in the supplemental material) and expression of high levels of GFP in sporozoites, similar to that in the Pbfluspo line (11), which was used as a WT control.

We first examined the WT (Pbfluspo) parasites at day 17 and day 22 after mosquito infection (Fig. 5B). Parasites could be detected in three different compartments, the midgut, the salivary glands, and the wings, the latter apparently reflecting the presence of parasites in the hemocoel (Fig. 5B). In sharp contrast, *siap-1*(−)/*GFP* parasites were observed only in the midguts and wings of infected mosquitoes but not in the salivary glands (Fig. 5B). Closer examination of the midguts of *siap-1*(−)/*GFP* parasite-infected mosquitoes on day 21 postinfection revealed the presence of numerous oocysts, most of

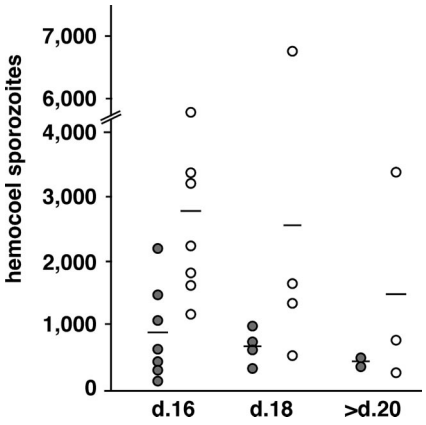

FIG. 6. Quantitative assessment of *siap-1*(−) sporozoite release into the mosquito hemocoel. Shown are quantifications of hemocoel sporozoites per infected mosquito for *siap-1*(−) (gray circles) and WT (white circles) parasites. The bars represent the mean values.

which quickly ruptured after dissection of the midgut, releasing high numbers of sporozoites (Fig. 5C). This is consistent with a defect in egress from oocysts in *SIAP-1*-deficient parasites. However, this defect is not complete, since *siap-1*(−)/*GFP* sporozoites could be found in the hemocoel, as demonstrated by closer examination of the wings of infected mosquitoes (Fig. 5D). These sporozoites were either nonmotile or displayed a limited nonproductive motility (data not shown), as typically observed with oocyst-derived sporozoites.

To provide a quantitative assessment of *siap-1*(−) sporozoite egress, we isolated hemolymph from infected mosquitoes and determined the numbers of hemocoel sporozoites (Fig. 6). We consistently recovered *siap-1*(−) sporozoites from hemocoel, but the numbers were typically lower compared to those of WT parasite-infected mosquitoes. This result differs markedly from *TRAP* knockout sporozoites, which egress normally but are impaired in their capacity to invade salivary glands, resulting in a significant accumulation of hemocoel sporozoites (10). Lower hemocoel sporozoite numbers of the *siap-1*(−) parasites indicate a defect in exiting oocysts. However, the *siap-1*(−) phenotype is an intermediary between the WT and the ones observed for egress mutants, e.g., the *CSP* region II mutant and the Pb*sera5*/*ecp1*(−) parasites (1, 23). Collectively, these data confirm that deletion of *SIAP-1* causes a partial defect in the egress from oocysts and indicate an additional effect on invasion of salivary glands.

We next examined the gliding locomotion of the *siap-1*(−) sporozoites (Fig. 7). Midgut-associated sporozoites isolated from *siap-1*(−) parasite-infected mosquitoes are indistinguishable from sporozoites isolated from WT parasite-infected mosquitoes and display infrequent, nonproductive motility. Continuous gliding locomotion, as seen in a proportion of WT hemocoel sporozoites, was completely absent from *siap-1*(−) sporozoites, indicating an important role for *SIAP-1* in this process.

Finally, we investigated the role of *SIAP-1* in transmission of sporozoites to the mammalian host (Table 1). Rats were exposed to the bites of mosquitoes infected with WT or *siap-1*(−) parasites. Subsequently, animals were checked daily by blood smear examination to detect the appearance of a blood stage infection. In contrast to WT parasites, which induced parasitemia in all exposed animals, none of the rats exposed to *siap-1*(−) parasites developed a patent blood stage infection (Table 1). We obtained the same result in C57/BL6 mice. All mice exposed to the bites of 20 mosquitoes infected with *siap-1*(−) parasites ($n = 2$) or *siap-1*(−)/*GFP* parasites ($n = 5$) remained blood smear negative. Furthermore, we bypassed natural transmission and injected mice with *siap-1*(−) sporozoites isolated from salivary glands, hemocoel, or midguts of infected mosquitoes. Infected animals typically remained blood smear negative (Table 1). As observed previously with the *trap*(−) mutant (17), only very high inocula, i.e., 50,000 salivary gland sporozoites or 1 million midgut-associated sporozoites, induced patently infected animals.

Collectively, our results demonstrate that *SIAP-1* plays a dual role in parasites' egress from midgut-associated oocysts and sporozoite colonization of salivary glands. Both cellular functions are directly linked to sporozoite locomotion, a vital

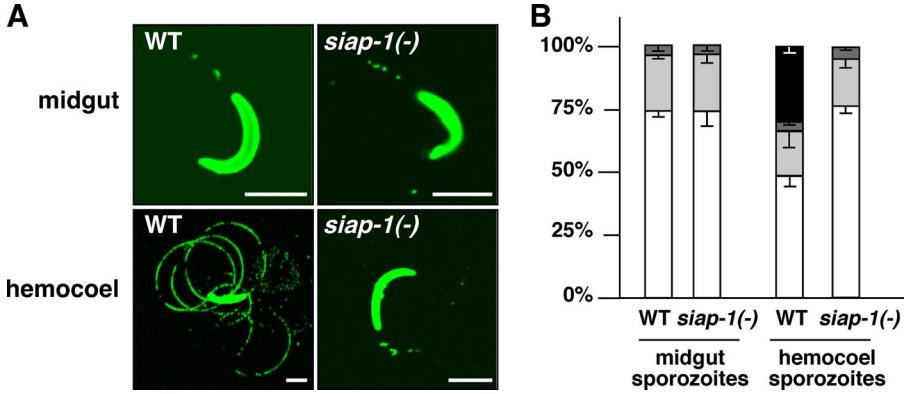

FIG. 7. Defective gliding locomotion in *siap-1*(−) sporozoites. (A) Representative immunofluorescence pictures of sporozoites isolated from *Anopheles* midguts or hemocoels. Sporozoites were deposited onto coated coverslips, and trails were visualized with the anti-circumsporozoite protein (CSP) antibody. Note that *siap-1*(−) hemocoel sporozoites lack productive motility and are indistinguishable from midgut-associated sporozoites. (B) Quantification of the WT and *siap1*(−) motility patterns. Shown is the percentage of nonmotile, i.e., detached (white) and attached (light gray), sporozoites and sporozoites that display nonproductive (dark gray) and productive (black) motility. In contrast to WT sporozoites that mature upon egress to the mosquito hemocoel, *siap-1*(−) parasites remain nongliding.

TABLE 1. In vivo infectivity of *siap-1*(−) and WT parasites

Location of sporozoite population	Parasite population	Method of inoculation or no. of sporozoites[a]	No. of infected animals/ inoculated animals	Prepatent period (days)[b]
Salivary gland	*siap-1*(−)	Mosquito bite	0/4	NA
	WT	Mosquito bite	8/8	3.5
	siap-1(−)	50,000	1/1	6
	siap-1(−)	10,000	0/5	NA
	WT	10,000	2/2	3.5
Hemocoel	*siap-1*(−)	10,000	1/4	6
	siap-1(−)	5,000	0/3	NA
	WT	1,000	10/10	4.7
Midgut	*siap-1*(−)	1,000,000	1/1	5
	siap-1(−)	400,000	1/2	7
	siap-1(−)	100,000	1/7	7
	WT	100,000	10/10	5.4

[a] Young Sprague-Dawley rats were injected intravenously with indicated numbers of sporozoites or exposed to the bites of 5 to 10 infected mosquitoes at days 17 to 20 after mosquitoes were infected.
[b] NA, not applicable.

parasite activity that is abolished in *SIAP-1* loss-of-function lines. These defects result in a complete block of sporozoite transmission from highly infected mosquitoes.

DISCUSSION

In this study, we identified the first conserved gene among apicomplexan hemoprotozoa that plays an essential role in sporozoite transmission to the mammalian host. *SIAP-1* loss-of-function sporozoites display a specific defect in sporozoite maturation. *Anopheles* mosquitoes infected with *siap-1*(−) parasites cannot transmit malaria to susceptible rodents, despite the normal formation of sporozoites in their midguts. Mutant parasites fail to mature, as seen by the lack of continuous gliding locomotion in hemocoel sporozoites and colonization of the final target organ, the salivary glands. This phenotype correlates with a transient accumulation in midgut oocysts and is reminiscent of the previously described egress mutants (1, 23). However, a direct role in oocyst rupture is unlikely because *siap-1*(−) sporozoites were consistently recovered outside the midgut.

One possible function of *SIAP-1* is a role in parasite locomotion. This notion is supported by the complete absence of trail formation and entry into salivary glands. In addition, tagging of the endogenous *SIAP-1* copy revealed a striking distribution with apical polarization and accumulation to additional specific areas. Intriguingly, these *SIAP-1*-positive patches remain constant upon sporozoite motility. Therefore, an immediate role, for instance in association with TRAP family invasins, in rearward distribution of tight junctions between sporozoite receptors and the substratum is unlikely. Because of the paucity of typical microfilaments in extracellular stages of apicomplexan parasites we could not address whether the composition of the motor machinery in vivo is altered in *siap-1*(−) sporozoites. The distribution pattern of Pb*SIAP-1*/*mCherry* combined with the absence of trail formation suggest that SIAP-1 may localize to structures located under the sporozoite surface and may be involved in gliding motility, possibly by interacting with the inner membrane complex. Alternatively, we cannot exclude an extracellular function, perhaps in preparation for active locomotion. In *P. falciparum*, SIAP-1 is processed and released into the supernatant upon incubation at 37°C (14), a feature shared with the apical membrane antigen 1 and TRAP. Presently, it is unknown where SIAP-1 is clipped. Due to the presence of a predicted cleavable signal sequence, we fluorescently tagged SIAP-1 at the carboxy terminus. Hence, we may only be able to visualize the unprocessed full-length protein, and localization of the mature form may differ, including dissociation into the extracellular milieu and deposition onto trails.

At this stage, we cannot formally exclude a protective role of SIAP-1 against clearance in mosquitos. Sporozoites that fail to reach and penetrate the salivary glands are quickly cleared by the mosquito immune system (22). Previous studies with *trap*(−) and *maebl*(−) parasites showed that a block in life cycle progression translates into accumulation of hemocoel sporozoites. Absence of *SIAP-1* on the sporozoite surface may render sporozoites more accessible to the mosquito innate immune system, resulting in enhanced clearance from the mosquito hemocoel.

Our results with *siap-1*(−) parasites clearly demonstrate that *SIAP-1* is required for efficient egress from oocysts and also for invasion of the mosquito salivary glands. In particular, using a novel approach that allows sensitive detection of fluorescent parasites in whole infected mosquitoes, we could show that a proportion of *siap-1*(−) sporozoites could exit from oocysts and access the hemocoel. Nevertheless, these parasites were not able to efficiently invade salivary glands. We hypothesize that the defect in motility in *siap-1*(−) sporozoites is responsible for the dual defect in egress from oocysts and invasion of salivary glands, resulting in a complete block in sporozoite transmission to the vertebrate host.

Apicomplexan sporogony in ticks differs largely from *Plasmodium* sporozoite formation in *Anopheles* mosquitoes. For instance, *Babesia* and *Theileria* sporozoite formation is initiated after kinete invasion of salivary glands and occurs inside a multinucleated sporoblast/sporont residing in a hypertrophied salivary gland cell. After exiting the sporoblast, sporozoites can be directly injected with the saliva into the vertebrate host, largely omitting the need for sporozoite-encoded proteins that function in the tick vector. Therefore, functional orthologs of *Plasmodium TRAP* and/or *MAEBL* may instead be expressed by the motile kinete. *SIAP-1* stands out as it appears to be structurally conserved across apicomplexan hemoprotozoa and may play similar roles in the final maturation steps of *Babesia* and *Theileria* sporozoites. Potential roles in sporozoite exit from the sporoblast or sporont and gliding locomotion will be difficult to address by genetic approaches in these parasites. Expression profiling during the parasite life cycles and complementation of the *siap-1*(−) phenotypes described in this study will reveal the degree of similarity between the orthologous genes.

Ultimately, identifying the conserved cellular roles of *SIAP-1* will provide important insights into basic principles of sporozoite biology and of arthropod-borne parasitic diseases.

ACKNOWLEDGMENTS

We thank Marion Steinbuechel for assistance with WT parasite-infected mosquito experiments, Diana Scheppan for assistance with whole mosquito pictures, and Kristin Götz for technical assistance.

This work was supported in part by grants from the research focus Tropical Medicine Heidelberg of the Medical Faculty of Heidelberg University, the Deutsche Forschungsgemeinschaft (SFB 544; no. B10), the European Commission (BioMalPar; no. 23), the Joachim Siebeneicher Foundation and the Chica and Heinz Schaller Foundation. O.S. is a recipient of a Marie Curie Intra-European Fellowship and an EMBO Long-Term Fellowship.

REFERENCES

1. **Aly, A. S., and K. Matuschewski.** 2005. A malarial cysteine protease is necessary for *Plasmodium* sporozoite egress from oocysts. J. Exp. Med. **202:**225–230.
2. **Doolan, D. L., S. Southwood, D. A. Freilich, J. Sidney, N. L. Graber, L. Shatney, L. Bebris, L. Florens, C. Dobano, A. A. Witney, E. Appella, S. L. Hoffman, J. R. Yates III, D. J. Carucci, and A. Sette.** 2003. Identification of *Plasmodium falciparum* antigens by antigenic analysis of genomic and proteomic data. Proc. Natl. Acad. Sci. USA **100:**9952–9957.
3. **Frischknecht, F.** 2007. The skin as interface in the transmission of arthropod-borne pathogens. Cell. Microbiol. **9:**1630–1640.
4. **Frischknecht, F., P. Baldacci, B. Martin, C. Zimmer, S. Thiberge, J. C. Olivo-Marin, S. L. Shorte, and R. Ménard.** 2004. Imaging movement of malaria parasites during transmission by *Anopheles* mosquitoes. Cell. Microbiol. **6:**687–694.
5. **Janse, C. J., B. Franke-Fayard, G. R. Mair, J. Ramesar, C. Thiel, S. Engelmann, K. Matuschewski, G. J. van Gemert, R. W. Sauerwein, and A. P. Waters.** 2006. High efficiency transfection of *Plasmodium berghei* facilitates novel selection procedures. Mol. Biochem. Parasitol. **145:**60–70.
6. **Kaiser, K., K. Matuschewski, N. Camargo, J. Ross, and S. H. Kappe.** 2004. Differential transcriptome profiling identifies *Plasmodium* genes encoding pre-erythrocytic stage-specific proteins. Mol. Microbiol. **51:**1221–1232.
7. **Kappe, S., T. Bruderer, S. Gantt, H. Fujioka, V. Nussenzweig, and R. Ménard.** 1999. Conservation of a gliding motility and cell invasion machinery in Apicomplexan parasites. J. Cell Biol. **147:**937–944.
8. **Kariu, T., M. Yuda, K. Yano, and Y. Chinzei.** 2002. *MAEBL* is essential for malarial sporozoite infection of the mosquito salivary gland. J. Exp. Med. **195:**1317–1323.
9. **Matuschewski, K.** 2006. Getting infectious: formation and maturation of *Plasmodium* sporozoites in the *Anopheles* vector. Cell. Microbiol. **8:**1547–1556.
10. **Matuschewski, K., A. C. Nunes, V. Nussenzweig, and R. Ménard.** 2002. *Plasmodium* sporozoite invasion into insect and mammalian cells is directed by the same dual binding system. EMBO J. **21:**1597–1606.
11. **Natarajan, R., V. Thathy, M. M. Mota, J. C. Hafalla, R. Ménard, and K. Vernick.** 2001. Fluorescent *Plasmodium berghei* sporozoites and pre-erythrocytic stages: a new tool to study mosquito and mammalian host interactions with malaria parasites. Cell. Microbiol. **3:**371–379.
12. **Potocnjak, P., N. Yoshida, R. S. Nussenzweig, and V. Nussenzweig.** 1980. Monovalent fragments (Fab) of monoclonal antibodies to a sporozoite surface antigen (Pb44) protect mice against malarial infection. J. Exp. Med. **151:**1504–1513.
13. **Shaner, N. C., R. E. Campbell, P. A. Steinbach, B. N. Giepmans, A. E. Palmer, and R. Y. Tsien.** 2004. Improved monomeric red, orange and yellow fluorescent proteins derived from *Discosoma* sp. red fluorescent protein. Nat. Biotechnol. **22:**1567–1572.
14. **Siau, A., O. Silvie, J.-F. Franetich, S. Yalaoui, C. Marinach, L. Hannoun, G.-J. van Gemert, A. J. F. Luty, E. Bischoff, P. H. David, G. Snounou, C. Vaquero, P. Froissard, and D. Mazier.** 2008. Temperature shift and host cell contact up-regulate sporozoite expression of *Plasmodium falciparum* genes involved in hepatocyte invasion. PLoS Pathog. **4:**e1000121.
15. **Silvie, O., K. Goetz, and K. Matuschewski.** 2008. A sporozoite asparagine-rich protein controls initiation of *Plasmodium* liver stage development. PLoS Pathog. **4:**e1000086.
16. **Sinden, R. E., and K. Matuschewski.** 2005. The sporozoite, p. 169–190. *In* I. Sherman (ed.), Molecular approaches to malaria. American Society for Microbiology Press, Washington, DC.
17. **Sultan, A. A., V. Thathy, U. Frevert, K. J. Robson, A. Crisanti, V. Nussenzweig, R. S. Nussenzweig, and R. Ménard.** 1997. TRAP is necessary for gliding motility and infectivity of *Plasmodium* sporozoites. Cell **90:**511–522.
18. **Tewari, R., D. Rathore, and A. Crisanti.** 2005. Motility and infectivity of *Plasmodium berghei* sporozoites expressing avian *Plasmodium gallinaceum* circumsporozoite protein. Cell. Microbiol. **7:**699–707.
19. **Thathy, V., and R. Ménard.** 2002. Gene targeting in *Plasmodium berghei*. Methods Mol. Med. **72:**317–331.
20. **Tsuji, M., D. Mattei, R. S. Nussenzweig, D. Eichinger, and F. Zavala.** 1994. Demonstration of heat-shock protein 70 in the sporozoite stage of malaria parasites. Parasitol. Res. **80:**16–21.
21. **Vanderberg, J. P.** 1975. Development of infectivity by the *Plasmodium berghei* sporozoite. J. Parasitol. **61:**43–50.
22. **Vaughan, J. A., L. Hensley, and J. C. Beier.** 1994. Sporogonic development of *Plasmodium yoelii* in five anopheline species. J. Parasitol. **80:**674–681.
23. **Wang, Q., H. Fujioka, and V. Nussenzweig.** 2005. Exit of *Plasmodium* sporozoites from oocysts is an active process that involves the circumsporozoite protein. PLoS Pathog. **1:**e9.
24. **Wengelnik, K., R. Spaccapelo, S. Naitza, K. J. H. Robson, C. J. Janse, F. Bistoni, A. P. Waters, and A. Crisanti.** 1999. The A-domain and the thrombospondin-related motif of *Plasmodium falciparum* TRAP are implicated in the invasion process of mosquito salivary glands. EMBO J. **18:**5195–5204.